# Friction on adsorbed monolayers

Elizabeth D. Smith and Mark O. Robbins

*Department of Physics and Astronomy, The Johns Hopkins University, Baltimore, Maryland 21218*

Marek Cieplak

*Institute of Physics, Polish Academy of Sciences, 02-668 Warsaw, Poland*

Molecular-dynamics simulations and analytical calculations are used to investigate the mechanism of energy dissipation in monolayer films sliding across a substrate. An explanation is given for the viscous friction found experimentally in both fluid and incommensurate solid adsorbates, and for the observation that solids slide more easily than fluids. We show that anharmonic coupling of phonons in the adsorbed monolayer can account for the rate of energy dissipation seen in these experiments. [S0163-1829(96)04935-1]

## I. INTRODUCTION

Friction is a common force whose microscopic origins and dependencies are poorly understood.[1] Here we describe our work using molecular-dynamics (MD) simulations and perturbation theory to study the friction present in a simple system: a noble-gas adsorbate on a noble-metal substrate. Our interest in studying friction on a molecular level originates in recent experiments[2–7] and computer simulations[8,9] which have revealed some intriguing differences between the behavior of macroscopic and microscopic systems.

Figure 1 illustrates two types of frictional force law that are normally observed for macroscopic fluids and solids. We will refer to them as viscous and static. For viscous force laws, commonly associated with fluids, the friction $F$ is proportional to the relative velocity $v$ between the sliding materials. This can be written as

$$F = \frac{M}{\tau} v \qquad (1)$$

where $M$ is the total mass of the sliding object, and $\tau$ is the sliptime. The sliptime characterizes the rate of momentum transfer between the substrate and adsorbate. With viscous friction no force is needed to initiate motion. For static force laws one must overcome a threshold force before motion occurs. Static friction is typically observed when one macroscopic solid slides on another.

Recent investigations of friction by Krim and co-workers[3,4] use the quartz-crystal microbalance (QCM) to measure the friction between adsorbed gas atoms and a substrate. In these experiments, gas atoms, such as Kr, Xe, or Ar, condense onto the surface of a quartz-crystal oscillator covered by a (111) oriented noble-metal substrate such as Au or Ag. The added mass of the adsorbate and the dissipation due to friction shift and broaden the microbalance resonance peak. By measuring these changes, information about the form and magnitude of the frictional force can be obtained.

In this paper we will focus on the experimental data for the Kr/Au system.[3] As Kr adsorbs onto the Au surface, it begins to form islands of liquid. These islands grow until a full liquid monolayer exists. As more Kr is adsorbed, the liquid becomes more dense. Eventually the monolayer undergoes a phase change into a crystalline state that is incommensurate with the underlying Au substrate.

The results of Krim and co-workers experiments on Kr/Au and related systems were surprising.[3] Solid monolayers did not exhibit the static friction typical of macroscopic solids. Instead, both the liquid and solid phases of the adsorbate exhibited a viscous force law. The frictional force on a fluid monolayer was measured to be about three orders of magnitude weaker than that between Kr layers in a bulk fluid. The frictional force on solid monolayers was even weaker. Solids slid more easily than fluids.

To understand these results, we did computer simulations which mimicked the important properties of Krim and co-workers' experiments, and developed an analytical theory of friction due to anharmonic coupling between phonons.[10] For clarity, will first explain the analytical theory, then describe the simulation technique. Finally, we will explain how the simulation results relate to, and elucidate, the experimental results, and show that the analytical theory can describe them both.
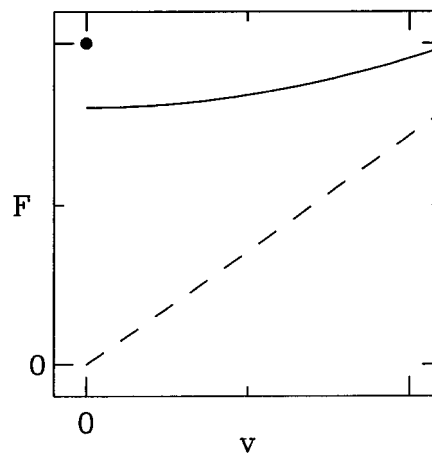


FIG. 1. A sketch of viscous and static force laws. With viscous friction (dashed line), the velocity and applied force are proportional. With static friction, a threshold force (filled circle) must be overcome before motion will occur (solid line).

## II. PERTURBATION THEORY FOR VISCOUS FRICTION

We treat the adsorbed monolayer as a two-dimensional elastic sheet which interacts with the substrate potential. The elastic sheet responds to the substrate potential, producing density modulations. If the substrate moves, the deformation induced by the substrate will try to follow the potential. In the process, some of the energy stored in the modulations will be transferred into other phonons modes due to anharmonicity. Our use of perturbation theory to analyze the dissipation associated with this transfer of energy is analogous to Sneddon, Cross, and Fisher's study of charge-density-wave conduction at large electric fields.[11] It is also similar to Sokoloff's[12] calculation for semi-infinite solids, but is not restricted to ideal crystalline layers.

The substrate potential $U(\mathbf{r},t)$ produces a force $\mathcal{F}(\mathbf{r},t) = -\nabla U(\mathbf{r},t)$ in the plane of the monolayer. The microscopic expression for the average power dissipated due to work on the adsorbed layer is

$$P = \lim_{T\to\infty} \frac{1}{T} \int_0^T dt \int d^2r \, \mathcal{F}(\mathbf{r},t) \cdot \mathbf{j}(\mathbf{r},t), \qquad (2)$$

where $\mathbf{j}(\mathbf{r},t)$ is the number current density of adsorbate atoms. Particle conservation requires $\nabla \cdot \mathbf{j}(\mathbf{r},t) = -dn(\mathbf{r},t)dt$, where $n(\mathbf{r},t)$ is the number density. Integrating Eq. (2) by parts yields

$$P = \lim_{T\to\infty} \frac{-1}{T} \int_0^T dt \int d^2r \, U(\mathbf{r},t) \frac{d}{dt} n(\mathbf{r},t). \qquad (3)$$

In the case of interest, the substrate is a crystal which is much more rigid than the adsorbed layer, and the motion of substrate atoms around lattice sites can be neglected. So $U(\mathbf{r},t)$ is a periodic potential that only has Fourier components at the substrate's reciprocal-lattice vectors, $\mathbf{G}_k$. As the substrate moves relative to the adsorbate with velocity $\mathbf{v}$, $U(\mathbf{G}_k,t)$ oscillates with frequency $\omega = \mathbf{v}\cdot\mathbf{G}_k$. Thus

$$U(\mathbf{r},t) = \sum_k U(\mathbf{G}_k)\exp[i\mathbf{G}_k\cdot(\mathbf{r}-\mathbf{v}t)]. \qquad (4)$$

We assume that the potential $U(\mathbf{q},\omega)$ is small enough that the number density responds linearly,

$$n(\mathbf{q},\omega) = -\alpha(\mathbf{q},\omega)U(\mathbf{q},\omega), \qquad (5)$$

$$n(\mathbf{r},t) = -\sum_k \alpha(\mathbf{G}_k,\mathbf{v}\cdot\mathbf{G}_k)U(\mathbf{G}_k)\exp[i\mathbf{G}_k\cdot(\mathbf{r}-\mathbf{v}t)]. \quad (6)$$

Using Eqs. (4) and (6) in Eq. (3), the power can then be expressed as

$$P = A_{\mathrm{ad}}\sum_k (-i\mathbf{G}_k\cdot\mathbf{v})U(-\mathbf{G}_k)\alpha(\mathbf{G}_k,\mathbf{v}\cdot\mathbf{G}_k)U(\mathbf{G}_k), \quad (7)$$

where $A_{\mathrm{ad}}$ is the area of the adsorbate film. Since $n(\mathbf{r},t)$ and $U(\mathbf{r},t)$ are real, $\alpha(\mathbf{q},\omega) = \alpha^*(-\mathbf{q},-\omega)$. This can be used to rewrite the power as

$$P = A_{\mathrm{ad}}\sum_k |U(\mathbf{G}_k)|^2 (\mathbf{G}_k\cdot\mathbf{v})\mathrm{Im}[\alpha(\mathbf{G}_k,\mathbf{G}_k\cdot\mathbf{v})]. \qquad (8)$$

Linear-response theory can only treat viscous friction [Eq. (1)]. In this case the macroscopic expression for the dissipated power is

$$P = \mathbf{F}\cdot\mathbf{v} = \frac{Mv^2}{\tau}. \qquad (9)$$

We can calculate $\tau$ by equating the microscopic, [Eq. (8)] and macroscopic [Eq. (9)] expressions for the power. The result can be written as

$$\frac{1}{\tau} = \sum_k |U(\mathbf{G}_k)|^2 |\hat{\mathbf{G}}_k\cdot\hat{\mathbf{v}}|^2 |\mathbf{G}_k|^2 \mathrm{Im}\left[\frac{A_{\mathrm{ad}}\alpha(\mathbf{G}_k,\mathbf{G}_k\cdot\mathbf{v})}{M\mathbf{G}_k\cdot\mathbf{v}}\right]. \qquad (10)$$

The sliptime can be reexpressed in terms of measurable equilibrium properties. If the adsorbed layer is incommensurate with the substrate, then the density modulations are directly related to the static structure factor $S(\mathbf{q})$ that would be measured in a scattering experiment:

$$\frac{S(\mathbf{q})}{N_{\mathrm{ad}}} = \left|\frac{A_{\mathrm{ad}}}{N_{\mathrm{ad}}}n(\mathbf{q},0)\right|^2 = \left|\frac{A_{\mathrm{ad}}}{N_{\mathrm{ad}}}\alpha(\mathbf{q},0)\right|^2 |U(\mathbf{q},0)|^2, \quad (11)$$

where $N_{\mathrm{ad}}$ is the number of adsorbate atoms. Thus Eq. (10) can be written as

$$\frac{1}{\tau} = \sum_k |\hat{\mathbf{G}}_k\cdot\hat{\mathbf{v}}|^2 \frac{S(\mathbf{G}_k)}{N_{\mathrm{ad}}} \frac{1}{t_{\mathrm{ph}}(\mathbf{G}_k,\mathbf{G}_k\cdot\mathbf{v})}, \qquad (12)$$

where the effective phonon lifetime $t_{\mathrm{ph}}$ is defined by

$$t_{\mathrm{ph}}(\mathbf{q},\omega) \equiv \frac{m}{\bar{n}|\mathbf{q}|^2} \frac{\omega|\alpha(\mathbf{q},0)|^2}{\mathrm{Im}[\alpha(\mathbf{q},\omega)]}. \qquad (13)$$

Here $m = M/N_{\mathrm{ad}}$ is the adsorbate particle mass, and $\bar{n} = N_{\mathrm{ad}}/A_{\mathrm{ad}}$ is the number density. As shown in the Appendix, this expression reduces to the usual phonon lifetime for underdamped phonons when $v$ is much less than the sound velocity. Friction studies are almost always in this low velocity limit.

The only possible dependence of $\tau$ on the direction of sliding lies in $|\hat{\mathbf{G}}\cdot\hat{\mathbf{v}}|$. For substrates with square or hexagonal symmetry, the sum over symmetrically equivalent reciprocal-lattice vectors always gives a scalar, and $\tau$ is independent of sliding direction. We will see in Sec. III that the potential is dominated by the shortest reciprocal-lattice vectors for the cases of interest.[13] For the hexagonal symmetry of the fcc(111) surface used in experiments, summing over the six shortest reciprocal-lattice vectors gives

$$\frac{1}{\tau} = \frac{3S(G)}{N} \frac{1}{t_{\mathrm{ph}}}. \qquad (14)$$

For a square lattice the prefactor equals 2 instead of 3.

Equation (14) reveals that the sliptime is determined by two equilibrium properties: the structure factor and the phonon lifetime. The size of the normalized structure factor $S(\mathbf{G})/N$ describes how much the adsorbate deforms to match the periodic substrate potential, and is proportional to the energy of this deformation. The inverse phonon lifetime $1/t_{\mathrm{ph}}$ is a measure of the rate at which energy stored in this deformation, or frozen phonon, is transferred to other

phonons. The frictional drag $1/\tau$ is proportional to both the energy stored in the deformation and the rate at which it couples anharmonically to other phonon modes.

## III. SIMULATIONS

### A. Potentials

The interaction between two noble-gas adsorbate atoms separated by a distance $r$ is well described by the Lennard-Jones potential

$$V(r) = 4\epsilon \left[ \left( \frac{\sigma}{r} \right)^{12} - \left( \frac{\sigma}{r} \right)^{6} \right]. \quad (15)$$

The minimum in the potential occurs at $r_{min} = 2^{1/6}\sigma$ with a minimum energy of $\epsilon$. The results of our simulations are expressed in terms of $\epsilon$, $\sigma$, and the characteristic time $t_0 = \sqrt{m\sigma^2/\epsilon}$. For noble gases,[14] the value of $\epsilon/k_B$ typically ranges from 30 to 230 K, and $\sigma$ ranges from 2.75 to 4.00 Å. For the Kr-Kr interaction in the simulations of Kr on Au, we used $\epsilon/k_B = 201.9$ K and $\sigma = 3.57$ Å.[15] Hence the characteristic time scale of atomic motion was $t_0 = 2.5$ ps.

The experimental substrates were noble metals that are much more rigid than the adsorbed layers. In this limit, Thompson and Robbins[9] found that the friction between two materials is not greatly affected if the substrate atoms are kept at lattice sites. In our simulations we used an adsorbate-substrate potential that models the substrate as fixed atoms. We will discuss the implications of this below. An important advantage is that the corrugation, or variation of the potential within the plane of the surface, can be changed without varying the adsorption energy. Because of this we were able to study the effect of corrugation on friction.

The interaction potential $V_{sub}$ between an adsorbate atom and a rigid substrate can be expressed as a Fourier expansion in the reciprocal-lattice vectors of the substrate surface,

$$V_{sub}(\mathbf{x},z) = \left[ V_0(z) + f \sum_i V_i(z) \sum_j \cos(\mathbf{G}_{ij} \cdot \mathbf{x}) \right], \quad (16)$$

where $\mathbf{x}$ is the position within the plane of the substrate, $z$ is the distance above the first layer of substrate atoms, and $\mathbf{G}_{ij}$ is the $j$th reciprocal-lattice vector in the $i$th shell of symmetrically related vectors. The coefficients $V_i$ were evaluated by Steele[13] for a Lennard-Jones potential with energy and length scales $\epsilon'$ and $\sigma'$. For Kr on Au we used $\epsilon'/\epsilon = 1.19$ and $\sigma'/\sigma = 0.97$. The adsorption energy is determined by $V_0$, while the corrugation is determined by $V_i$ for $i > 0$. We introduced the parameter $f$ to be able to vary the corrugation of the substrate without changing the adsorption energy.

In our simulations we used Steele's coefficients $V_i$ with $i = 0 \leqslant 5$ for a fcc(111) substrate. However, the dominant term comes from the first shell, $i = 1$, which contains the six shortest wave vectors. These vectors have a length of $4\pi/\sqrt{3}d_{nn}$, where $d_{nn} = 2.885$ Å is the nearest-neighbor spacing in the Au substrate. The corrugation due to wave vectors in the next closest shell is two orders of magnitude smaller for the range of $z$ where the density of Kr atoms is appreciable. Shells that are further out make successively weaker contributions to the potential.

Although Steele evaluated $V_n$ for a Lennard-Jones potential, the true substrate potential is more complicated. Delocalized electrons in a metal substrate weaken the corrugation, but not the adsorption energy. Thus for Kr on Au the full corrugation of a Lennard-Jones potential ($f = 1$) is inappropriate. Helium scattering studies[16] show that an appropriate value of $f$ for a He on Ag system is about 0.1 or 0.2. Although Au and Ag are about the same size, we expect the corrugation of Kr on Au to be smaller because Au is less interactive, and larger Kr atoms do not get as close to the substrate surface as He atoms do. We will show that the value of $f$ needed to make our simulation data consistent with experiments is about 0.03.

The adsorbate atoms were kept from floating too far above the substrate by the addition of a hard-wall potential at a height of $8\sigma$ to $10\sigma$ above the substrate. In equilibrium, almost all of the atoms were on the surface, and the position of the wall was irrelevant. Periodic boundary conditions were imposed in the plane of the substrate. The fcc(111) substrate had dimensions $L_x = Ld_{nn}$ by $L_y = (\sqrt{3}/2)Ld_{nn}$ with $L = 10$ or 20. These dimensions represent substrate surfaces comprised of $N_{sub} = L^2 = 100$ or 400 Au atoms. Most data shown are for $N_{sub} = 400$.

Equilibrium initial conditions were created by the following procedure. We began by placing 5 or 10 atoms at random positions in the volume above the substrate. During an initial $200t_0$ equilibration period, these atoms condensed onto the substrate of area $A$ and diffused to form a compact island containing $N_{ad}$ atoms. The coverage $N_{ad}/A$ was gradually increased by adding 5 or 10 atoms at random positions, and allowing the system to evolve a further $200t_0$ or more. The addition of particles was repeated until the monolayer was so dense that several atoms were forced into a second layer. Friction measurements could be made at any stage of coverage after the corresponding equilibration period. We also tried other startup methods, and found that they resulted in similar final states after equilibration.

### B. Measurements of the sliptime $\tau$

The frictional force was measured either by applying a constant force to the adsorbed atoms or by oscillating the substrate. In constant force simulations, the substrate remains at rest, and an equal force $F$ is applied to each adsorbate atom in the first monolayer. This force starts at zero, and is ramped to its final value over $100t_0$. The force is then held constant for another $2000t_0$, and the steady-state velocity of the adsorbate, $v$, is measured.

If the friction force is of a viscous form, then the applied force is related to the measured velocity by Eq. (1), and a plot of $v$ vs $F$ allows us to calculate $\tau$. If the adsorbate-substrate interaction follows a static force law, the velocity is zero until unless the applied force is larger than the threshold or static friction force $F_s$.

A second type of simulation closely mimicked Krim and co-workers' experiments.[3,4] In quartz-crystal microbalance experiments, the substrate oscillates in the $x$-$y$ plane beneath the adsorbate. Assuming that a viscous force law applies, Krim and Widom[2] showed that the shift and broadening of the microbalance resonance frequency can be related to the

real and imaginary components, respectively, of the force on the substrate from the adsorbate. These components can in turn be related to the sliptime $\tau$.

In our simulations, the substrate's position was varied as $x_{sub} = A \sin \omega t$, resulting in a substrate velocity of $v_{sub} = A \omega \cos \omega t$. Assuming a viscous force law, the velocity of the adsorbate is

$$v_{ad} = \frac{v_{sub}}{1 + i \omega \tau} . \tag{17}$$

We determined the real and imaginary parts of $v_{ad}$ averaged over 20 or more periods. If the force law is indeed viscous, both real and imaginary components of $v_{ad}(\omega)$ should be fit by the single unknown $\tau$. To test this, we compared values of $\tau$ from two independent equations:

$$\omega \tau_1 = \frac{\mathrm{Im}(v_{ad}(\omega))}{\mathrm{Re}(v_{ad}(\omega))}, \tag{18}$$

$$\omega \tau_2 = \left( \frac{|v_{sub}|^2}{|v_{ad}|^2} - 1 \right)^{1/2} . \tag{19}$$

Deviations from a viscous force law can also be determined from measurements of the harmonic response at different displacement amplitudes $A$ and frequencies $\omega$.[17] In experiments, it is difficult to vary these parameters over a large range. However, such studies are possible when doing simulations. For a nonviscous form of the force, such as static friction, $\tau$ would be dependent on $A$ and $\omega$, and there would be higher harmonics of the oscillation frequency in $v_{ad}$. To verify that we were in a viscous regime, we checked that the velocity of the adsorbate did not contain such harmonics, and in Sec. IV we discuss results which show that the sliptime is independent of $A$ and $\omega$.

### C. Thermostat

Frictional dissipation causes the adsorbate to heat up as sliding occurs. The temperature does not rise significantly in experiments, because heat flows into the substrate. This can not happen with the rigid solid of our simulations. In order to simulate heat flow out of the system, we coupled a component of the velocity to a heat bath by adding damping and a Langevin noise term.[18,19] The component $v_{\perp}$ was chosen to be perpendicular to the direction of motion $\hat{x}$, in order to minimize the effect of the thermostat on the frictional force. The results remained the same whether this component was in the adsorbate plane ($\hat{y}$) or perpendicular to the adsorbate ($\hat{z}$). If damping is applied in the $x$ direction, the total damping rate $1/\tau_{tot} = F/(Mv)$ is increased from $1/\tau$ to

$$\frac{1}{\tau_{tot}} = \frac{1}{\tau} + \frac{1}{\tau_{therm}}, \tag{20}$$

where $\tau_{therm}$ is the time scale for coupling to the heat bath.

For a viscous force law, the rate of energy dissipation per atom at mean velocity $v$ is $mv^2/\tau$. In steady state this equals the rate of flow into the heat bath. For $v=0$, damping and random noise maintain a thermal distribution with

$$\langle v_{\perp}^2 \rangle = \frac{k_B T}{m} \equiv v_T^2 . \tag{21}$$

When $\langle v_{\perp}^2 \rangle$ deviates from the equilibrium value, heat flows into the reservoir at a rate

$$\frac{m}{\tau_{therm}} \left( v_{\perp}^2 - \frac{k_B T}{m} \right) = \frac{k_B}{\tau_{therm}} \Delta T_{\perp} , \tag{22}$$

where $\Delta T_{\perp}$ is the difference between the effective temperature associated with $\langle v_{\perp}^2 \rangle$ and that of the bath. Equating this to the dissipation yields

$$\frac{\Delta T_{\perp}}{T} = \frac{\tau_{therm}}{\tau} \frac{v^2}{v_T^2} . \tag{23}$$

For $T = 0.385\epsilon$, corresponding to 77 K, $v_T = 0.62\sigma/t_0$. Values of $v^2/v_T^2$ are typically less than $10^{-2}$ in simulations and less than $10^{-8}$ in experiments. Therefore, the damping rate of the thermostat $1/\tau_{therm}$ can be much smaller than the intrinsic frictional damping $1/\tau$ without substantial heating of the adsorbate. Equation (20) implies that there would be little effect on the measurement of $\tau$ for such weak thermostats, even if coupling was applied in the $x$ direction. We confirmed that damping did not effect our results by comparing runs with different $1/\tau_{therm}$ and short microcanonical runs.

### D. Structure factor and phonon lifetime

The perturbation theory presented above points to two quantities as being fundamental: the static structure factor at $\mathbf{G}$, $S(\mathbf{G})$, and the phonon lifetime $t_{ph}$. The static structure factor $S(\mathbf{q})$ was calculated every $0.25t_0$ during the simulation and averaged over $1500t_0$. To obtain the $\omega = 0$ value for our finite systems, we subtracted the diffuse background from neighboring $\mathbf{q}$. Values obtained in this manner were consistent with values obtained from the relation $S(\mathbf{q}, \omega = 0)/N_{ad} = |n(\mathbf{q}, \omega = 0)|^2$.

To calculate the phonon lifetime via Eq. (13), we first evaluated $[\mathrm{Im}\alpha(\mathbf{G}, \omega)/\omega \mathrm{Re}\alpha(\mathbf{G}, \omega)]$, which equals $[\mathrm{Im}\alpha(\mathbf{G}, \omega)/\omega|\alpha(\mathbf{G}, 0)|]$ in the limit of small $\omega$, or equivalently $v \ll v_{sound}$ (see the Appendix). This quantity was determined by varying the corrugation factor $f$ sinusoidally in time with frequency $\omega$. The in-phase and out-of-phase components of the response $n(\mathbf{G}, \omega)$ were then measured. From Eq. (6) the ratio $\mathrm{Im}(n)/\omega \mathrm{Re}(n)$ is equal to $\mathrm{Im}(\alpha)/\omega \mathrm{Re}(\alpha)$.

To determine $|\alpha(\mathbf{G}, 0)|$, one needs to know the absolute strength of the corrugation. While the analytic calculation assumed a two-dimensional sheet, the value of $z$ that minimizes the potential varies substantially in the plane of the substrate. We found that atoms stayed near this minimum-energy surface. The value of $U(\mathbf{G}, \omega)$ was obtained from $U(\mathbf{x}, \bar{z}(\mathbf{x}), t)$, where $\bar{z}$ was the mean height of atoms at position $\mathbf{x}$ during an equilibrium run. The response $n(\mathbf{G}, \omega)$ was obtained by projecting atoms into the $x$-$y$ plane.
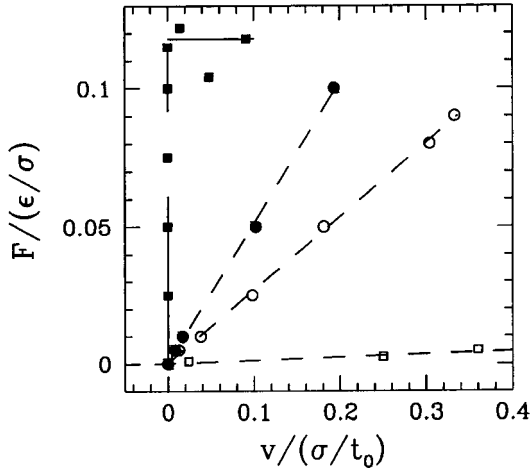
FIG. 2. Variation of steady-state velocity $v$ with force per atom $F$. Results for an incommensurate case that models Kr on Au ($\epsilon' = 1.19\epsilon$, $\sigma' = 0.97\sigma$, $f = 1$, $N_{ad} = 49$, and $N_{ad}/A_{surf} = 0.068$ Å$^2$) at $k_B T/\epsilon = 0.385$ (solid phase) and 0.8 (fluid phase) are shown by open and filled circles, respectively. Results for $\epsilon' = \epsilon$, $\sigma' = \sigma = 2^{1/6} d_{nn}$, $k_B T = 0.385\epsilon$, and $N_{ad} = 64$ are shown by squares. For $f = 0.3$ (closed squares) the adsorbate is a commensurate solid, and for $f = 0.1$ (open squares) the adsorbate is incommensurate.

## IV. RESULTS

### A. Constant force results

We began by using constant force simulations for a number of model adsorbate and substrate atoms to determine the conditions under which static and viscous force laws applied. The results showed that the structure of the adsorbate is the determining factor in the type of friction law exhibited. We found three types of structure: a liquid phase, a solid phase which was commensurate with the substrate, and a solid phase which was incommensurate with the substrate.

Figure 2 shows force vs velocity data for several different simulation conditions. Dense fluids (open circles) and incommensurate solids (filled circles) exhibited a viscous force law for all parameters tested. The circles in Fig. 2 indicate results from simulations of Kr on Au with a strong substrate corrugation ($f = 1$). As in the experimental work of Krim and co-workers,[3,4] the force on the solid phase is smaller than that on the fluid phase at the same velocity.

Commensurate solids exhibited a threshold force or static friction. As illustrated by the filled squares in Fig. 2, there was no motion until the applied force was larger than some yield force. For these data $d_{nn} = 2^{1/6}\sigma$, $\epsilon' = \epsilon$, and $f = 0.3$. When $f$ was lowered below 0.2, we found that the adsorbate underwent a structural change to an incommensurate solid, and the measured friction was viscous. The reason for this structural change is that the adsorbed layer is slightly compressed when locked into the commensurate structure. For $f = 0.3$ the substrate potential is strong enough to force the adsorbed layer into registry, but as $f < 0.2$ the adsorbed layer adopts the lower-density incommensurate phase favored by its internal interactions. The extra atoms are pushed into the second monolayer.

Many previous studies of friction have been based on the simple Frenkel-Kontorova (FK) model.[20,21] Like our model,

this model replaces the substrate by a periodic potential. It then models the adsorbate interactions as springs between nearest neighbors. Since the springs fix the topology of the layer, only crystalline phases can be studied. Also, there is no way for the adsorbate density to change since particles in one layer cannot move in or out of a second layer. For the usual case of harmonic springs ($t_{ph} \to \infty$), there is no damping due to coupling between phonons. Instead, an external damping term, like that in our thermostat, is added to the equations of motion.

The simplicity of the FK model makes it amenable to analytic treatments. When the spring lengths are naturally commensurate with the substrate, or pulled in to commensurability by the potential, a static friction law is found. This is because all the atoms move up and down over the periodic potential in phase. When the lengths are incommensurate, the atoms sample all phases of the potential at each instant, and there is no net energy barrier to motion. This leads to a viscous force law with $\tau$ equal to the external damping time. Some have argued that this implies incommensurate systems could slide with zero friction,[21] but the presence of anharmonic terms in any real potential will always lead to a finite friction force through Eq. (14).

### B. Oscillating substrate results

#### 1. Testing the premise of viscous friction

As stated above, in simulations of Kr on Au the structure of the adsorbate was either a fluid or an incommensurate solid. Both cases fall into the regime of viscous friction. We will first present some data that show the range of conditions over which we found Eqs. (18) and (19) to be valid. Then we will discuss results that support the analytical theory of Sec. II, and help explain the experimental results of Krim and co-workers.[3,4]

If the friction force is linear in the sliding velocity, then we expect only the first harmonic of the oscillation frequency to appear in the adsorbate velocity $v_{ad}$. Our results were consistent with this expectation. We found that the second and third harmonics were less than the calculated error. This error was typically less than 5% of the magnitude of the first harmonic.

As mentioned earlier, Eqs. (18) and (19) should independently give the same value for $\omega\tau$ if the force law is viscous. In Table I we show $\omega\tau$ data for solid and fluid phases at various substrate amplitudes. Equation (18) was used to calculate data in the column labeled $\omega\tau_1$, and Eq. (19) was used for $\omega\tau_2$. Also included in this table is the peak-to-peak slip distance $d_{slip}$, the distance the adsorbate slides with respect to the substrate. For substrate oscillation amplitudes $A$ less than $10\sigma$, the value of $\tau$ is constant. The two methods of calculating $\omega\tau$ are in agreement, although the statistical errors in $\omega\tau_2$ are larger at low $A$. We had originally thought that $\tau$ would depend on the sliding distance, because atoms must move by more than a lattice constant in order to sample a representative section of the surface. However, the different atoms in liquid and incommensurate layers sit at all possible positions relative to substrate atoms. As long as the substrate potential is a weak perturbation, the sliding distance is not important.

TABLE I. Values of $\omega\tau$, slip distance, and temperature increase $\delta T_x(\epsilon)$ for different substrate oscillation amplitudes at $\omega=0.0628$ and $f=0.5$. The two values $\omega\tau_1$ and $\omega\tau_2$ were obtained from Eqs. (18) and (19), respectively.

| Amplitude | Solid | | | | Fluid | | | |
|---|---|---|---|---|---|---|---|---|
| | $\omega\tau_1$ | $\omega\tau_2$ | $\delta T_x(\epsilon)$ | $d_{slip}(\sigma)$ | $\omega\tau_1$ | $\omega\tau_2$ | $\delta T_x(\epsilon)$ | $d_{slip}(\sigma)$ |
| 40 | 0.484(6) | 0.500(6) | 0.04 | 34.9(3) | 0.34(1) | 0.42(2) | 0.04 | 25.8(6) |
| 30 | 0.524(3) | 0.542(6) | 0.03 | 27.8(3) | 0.24(1) | 0.27(1) | 0.02 | 14.0(6) |
| 20 | 0.62(1) | 0.64(2) | 0.01 | 21.1(5) | 0.20(1) | 0.17(4) | 0.01 | 7.8(4) |
| 10 | 0.79(2) | 0.78(2) | 0.00 | 12.4(5) | 0.16(1) | 0.17(3) | 0.00 | 3.2(3) |
| 5 | 0.82(3) | 0.85(6) | 0.00 | 6.3(3) | 0.16(1) | 0.14(4) | 0.00 | 1.57(1) |
| 2.5 | 0.82(3) | 0.9(1) | 0.00 | 3.2(2) | 0.17(1) | 0.09 | 0.00 | 0.8(1) |
| 1.0 | 0.87(6) | 0.8(1) | 0.00 | 1.1(2) | 0.14(2) | – | 0.00 | 0.26(8) |
| 0.5 | | | | | 0.17(5) | – | 0.00 | 0.17(7) |

For larger amplitudes ($A>10\sigma$), $\tau_1$ and $\tau_2$ are slightly different, and both begin to deviate from the constant value found at smaller amplitudes. We attribute this change to the temperature increase reported in Table I. The rate at which work is done scales as the amplitude squared, and at high amplitudes the thermostat cannot remove the associated heat fast enough. The effective temperature rise of each component of the velocity was defined as $\Delta T_i=(m/k_B)\langle v_i^2\rangle-T$. The velocity in the $z$ direction was coupled to the heat bath directly. The coupling in this direction was strong enough to keep $\Delta T_z$ small. Kinetic energy in the $x$ and $y$ directions first had to be diverted to motion in the $z$ direction before being removed by the heat bath. Because coupling between different directions of motion takes time, the temperature in these directions is sometimes higher than desired. We include $\Delta T_x$ in Table I as a measure of how much extra heat was in the adsorbate. To confirm that the amplitude dependence is not intrinsic, we considered variations with frequency. The amount of heating scales as $\omega^2$. As expected, at lower frequencies the temperature and $\tau$ remain constant to larger amplitudes.

Viscous friction also implies that $\tau$ is independent of $\omega$. Table II gives $\omega\tau$ and $\tau$ for frequencies ranging between $0.0157/t_0$ and $0.2513/t_0$. The values of $\omega\tau$ were calculated using Eq. (18). Different amplitudes were used with different frequencies. Each amplitude was chosen such that the resulting adsorbate velocity would be large enough to measure accurately, and yet small enough to avoid heating problems. As expected for viscous friction, $\tau$ was constant within our error.

TABLE II. Values of $\omega\tau$ and $\tau$ at $f=0.5$ for different substrate oscillation frequencies.

| $\omega t_0$ | Solid | | Fluid | |
|---|---|---|---|---|
| | $\omega\tau$ | $\tau/t_0$ | $\omega\tau$ | $\tau/t_0$ |
| 0.2513 | 3.0(6) | 12(2) | 0.69(2) | 2.7(1) |
| 0.1257 | 1.6(1) | 13(1) | 0.36(2) | 2.9(2) |
| 0.0628 | 0.80(5) | 13(1) | 0.16(1) | 2.5(2) |
| 0.0314 | 0.39(7) | 12(2) | 0.08(1) | 2.5(3) |
| 0.0157 | 0.22(1) | 14(1) | 0.045(6) | 2.9(3) |

### 2. Dependence on corrugation and sliding direction

Having demonstrated that our system exhibits a viscous force law, we now turn to the verification of the form of the perturbation theory proposed in Sec. II. As explained there, $\tau$ should not depend on the direction of motion with respect to a fcc(111) substrate. This dependence was tested by varying the direction of motion over its full range in 10° increments. We saw no change in the value of $\tau$ which was greater than the 4% error in our calculations.

The analytical theory also predicts that $\tau\propto|U(\mathbf{G})|^{-2}\propto f^{-2}$. To test this we evaluated $\tau$ for systems with different corrugations. Figure 3 shows a log-log plot of $\tau$ vs $f$ for two coverages, $N_{ad}/A_{surf}=0.057$ and $0.070$ $\text{Å}^2$, that correspond to solid and fluid phases, respectively. Both sets of data are clearly linear with a slope of $-2$, as predicted by the analytic theory. Since small changes in $f$ result in large changes in $\tau$, determinations of $\tau$ can be used as a sensitive measurement of the substrate corrugation. Once again, the data in Fig. 3 show that solids (squares) always slide more easily than fluids (triangles) for a given corrugation. This observa-
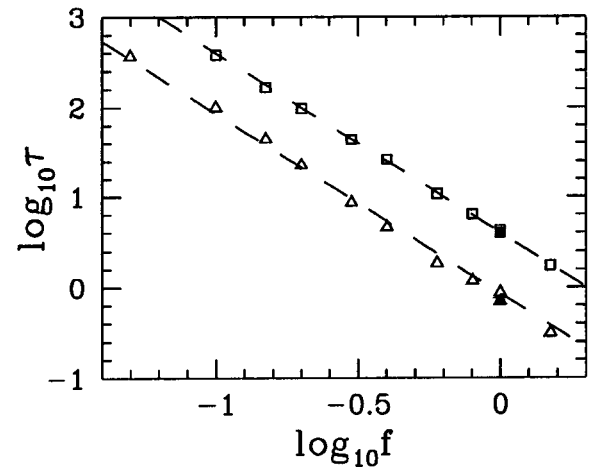


FIG. 3. Variation of $\tau$ with substrate corrugation $f$ at $N_{ad}/A_{surf}=0.057$ $\text{Å}^2$ (triangles), and $N_{ad}/A_{surf}=0.070$ $\text{Å}^2$ (squares), for a model of Kr on Au ($t_0=2.5$ ps). Open symbols are for oscillating substrate simulations that mimicked the QCM. Note that these are consistent with constant force measurements (filled symbols). Error bars are comparable to the symbol size.
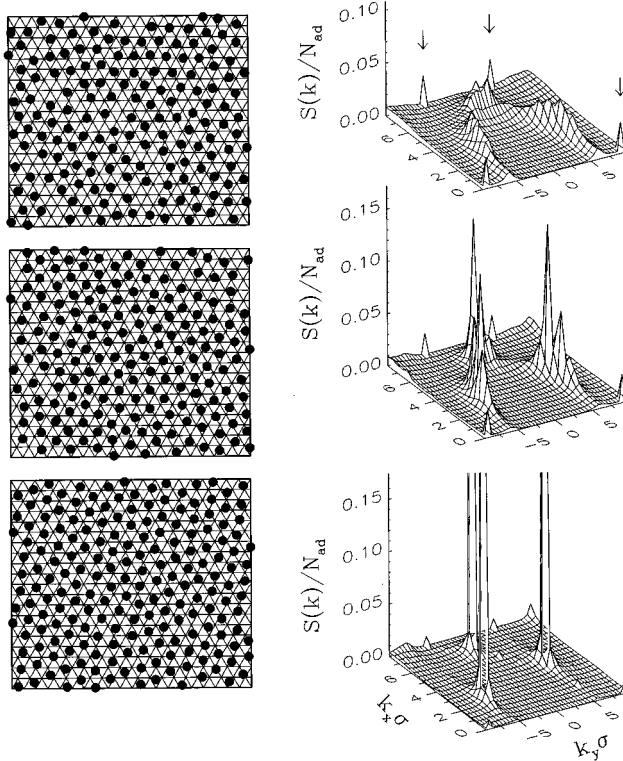
FIG. 4. Particle positions (left) and $S(\mathbf{k})/N_{ad}$ (right) are shown for three different coverages $N_{ad}/A_{surf}=0.057$ Å$^2$ (top), 0.062 Å$^2$ (middle), and 0.068 Å$^2$ (bottom). Circles show the location of Kr atoms. Arrow indicate $\mathbf{G}$. Au atoms sit at the vertices of the underlying triangular grid.

tion agrees with Krim and co-workers' finding that solid Kr slides more easily on Au than fluid Kr does.[3,4] Finally, since the solid and fluid curves scale in the same way, results for all $f$ in the viscous regime can be determined from variations in $\tau$ with temperature[22] or coverage at a single $f$.

### 3. Comparison with experimental data

We have done simulations at constant temperature, $0.385\epsilon/k_B=77$ K, for varying coverages in order to compare directly to experiments done by Krim and co-workers.[3,4] The adsorbate goes through structural changes as the coverage increases, and we measured these changes by the structure factor $S(\mathbf{k})$. At low coverages the adsorbate layer is comprised of small islands of fluid. As more particles are added, these islands grow larger, and finally coalesce to form a complete fluid monolayer at $N_{ad}/A_{surf}=0.055$ Å$^2$ ($N_{ad}/N_{surf}=0.40$). The top of Fig. 4 shows the real-space particle positions and $S(\mathbf{k})/N_{ad}$ for a typical fluid phase. The usual ring associated with a fluid $S(\mathbf{k})/N_{ad}$ plot is modulated by the underlying substrate. Notice the small peaks at the substrate's reciprocal lattice vectors $\mathbf{G}$. As the number of particles increases further, the fluid monolayer increases in density. The middle of Fig. 4 shows typical positions and $S(\mathbf{k})/N_{ad}$ for a dense fluid. At this coverage, the fluid ring in $S(\mathbf{k})/N_{ad}$ is extremely modulated by the substrate. A further increase in coverage and the adsorbate crystallizes into an incommensurate solid monolayer at $N_{ad}/A_{surf}=0.068$ Å$^2$ ($N_{ad}/N_{surf}=0.49$). At the bottom of Fig. 4 are the real-space particle positions and $S(\mathbf{k})/N_{ad}$ for a typical solid phase. As



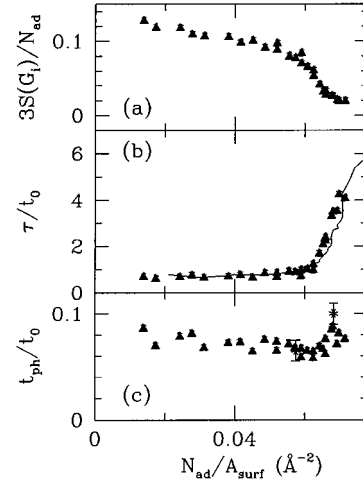FIG. 5. Simulation results (triangles) for (a) $3S(\mathbf{G})/N$ and (b) $\tau/t_0$ as a function of coverage $N_{ad}/A_{surf}$ for a model of Kr on Au at $T=77$ K ($=0.385\epsilon/k_B$) with $A_{surf}=2883$ Å$^2$ and $f=1$. The product of the two quantities is shown in (c). Equation (14) implies that this product equals $t_{ph}/t_0$. Error bars indicate directly determined values of $t_{ph}/t_0$. Experimental results (Ref. 3) for Kr on Au at 77 K are shown as a solid line in (b). These values of $\tau$ were normalized by $t_0$, and then divided by 1000. Calculated values of $\tau$ would increase by this factor if $f$ was reduced to about 0.03.

the coverage continues to increase, the adsorbate remains a solid whose density increases slightly.

An explanation of why solids slide more easily than fluids can be found in Fig. 4. At low coverages, up to the fluid monolayer, $S(\mathbf{G})/N_{ad}$ is relatively large, while in the solid phase, $S(\mathbf{G})/N_{ad}$ can barely be seen. Because of this decrease in $S(\mathbf{G})/N_{ad}$, Eq. 14 leads us to expect a corresponding increase in $\tau$. A plot of $3S(\mathbf{G})/N_{ad}$ vs coverage is shown in Fig. 5(a). The triangles in Fig. 5(b) show $\tau$ vs coverage as measured in our simulations. A comparison with Fig. 5(a) shows that indeed, as $S(\mathbf{G})/N_{ad}$ decreases with coverage, the sliptime $\tau$ increases.

Also in Fig. 5, it can be seen that $\tau$ has a constant low value until $N_{ad}/A_{surf}=0.055$ Å$^2$. This is expected since for all coverages from islands to fluid monolayers the density is a constant. Deviations from this constant value may occur for small islands if edge effects are important.

Equation (14) states that $\tau$ is inversely proportional to $S(\mathbf{G})$ and proportional to $t_{ph}$, the phonon lifetime. Using the measurements of $3S(\mathbf{G})/N$ and $\tau$, as plotted in Fig. 5, we have calculated the value of $t_{ph}$ implied by Eq. (14) and plotted it in Fig. 5(c). As seen in this plot, the phonon lifetime remains fairly constant as the coverage changes. The changes in $S(\mathbf{G})$ alone can account for the changes in $\tau$. As explained in Sec. III D, we have also determined $t_{ph}$ by independent means. The results are the points with error bars plotted in Fig. 5(c). The agreement between values of $t_{ph}$ measured in simulations and values predicted by perturbation theory allow us to conclude that the theory correctly accounts for the dissipation in our systems.

The changing of $\tau$ with coverage from a small value in the fluid phase to a large value in the solid phase is exactly the surprising change that Krim and co-workers saw in the Kr-Au experiments. By comparing our simulation data to

Krim and co-workers' data, we were able to estimate the corrugation of Kr on Au. Our data were taken at $f = 1.0$. Fitting to Krim and co-worker's data we estimate that the corrugation in the experiments is $f = 0.032$. As expected this value is slightly smaller than the corrugation measured by He scattering studies of Ag.[16] The excellent fit of simulation data to experimental data can be seen in Fig. 5(a), where data from Krim and co-workers' experiment have been plotted as a line. These data have been rescaled from a corrugation of 0.032 to a corrugation of 1.00, by multiplying $\tau$ by a constant factor of 1000.

## V. SUMMARY AND CONCLUSIONS

In this paper we have discussed simulations and analytic calculations which show how phonons can account for energy dissipation due to viscous friction between a substrate and an adsorbed monolayer. The analytical theory gives us Eq. (14), which relates equilibrium properties to the sliptime $\tau$. The results of computer simulations are in good agreement with experimental results for the Kr/Au system studied by Krim and co-workers,[3,4] and are quantitatively described by analytic perturbation theory.

Our perturbation theory and simulation results allow us to understand better why solids feel a smaller viscous frictional force than fluids. A monolayer solid is a rigid network of atoms that cannot deform itself readily to an external potential. A fluid layer though, can easily deform and lock itself to the substrate, thereby inhibiting its motion. Our theory uses $S(\mathbf{G})$ to relate this deformability to $\tau$. The difference in deformability is larger at $\mathbf{k} = \mathbf{G}$ than at $\mathbf{k} = \mathbf{0}$, because deformations at $\mathbf{k} = \mathbf{G}$ require only local atomic displacements while deformations at $\mathbf{k} = \mathbf{0}$ require changes in the average density.

Just as the substrate deforms the adsorbate, the adsorbate will deform the substrate. Since the structure factor scales as the square of the compressibility, and Au is about 100 times less compressible than Kr, the deformation of Au is negligible. This justifies our use of a rigid substrate. In other systems, where the compressibilities are more closely matched, deformations in both the substrate and adsorbate would need to be accounted for.

In our perturbation theory, the energy loss associated with friction occurs via anharmonic coupling of substrate-induced deformations to other phonons in the adsorbate. This is the only source of energy dissipation possible in our simulations, and can account for the frictional dissipation seen by Krim and co-workers.[3,4] Persson[23] has argued that adsorbate-substrate friction is dominated by electronic excitations. In his model these produce a damping force on each adsorbate atom that has the same form as our thermostat. As noted in Sec. III C, our thermostat did not effect $\tau$ because only velocities perpendicular to the direction of motion were damped. If Persson's electronic damping term is added in the sliding direction, all of our values of $1/\tau$ increase by the same constant amount as in Eq. (20). Then, in order to obtain quantitative agreement with experimental data at any given coverage, we would have to use a smaller $f$. Moreover, $f$ would need to vary with coverage in order to maintain the correct ratio between fluid and solid friction.

The work discussed here shows that phonons can be an important mechanism of energy dissipation due to friction.

More work needs to be done to ascertain the relationship of these results to macroscopic systems and to more complex microscopic systems. Solid macroscopic interfaces are almost always incommensurate. From the results reported here and work reported elsewhere,[21,24] one would then expect to observe viscous friction in almost all solid-solid systems. On the contrary, most solid systems exhibit a static force law. It is possible that surface roughness and other disorder plays an important role in the observed friction. Alternatively, the relatively high loads used in friction measurements may result in large enough values of the corrugation to put the system in a static friction regime.

## APPENDIX: CALCULATING THE PHONON LIFETIME

In this appendix we relate Eq. (13) to the usual phonon lifetime. We first solve for the response function $\alpha(\mathbf{q}, \omega)$. Newton's equation of motion for an elastic sheet can be written as

$$\frac{d}{dt}\frac{m}{\bar{n}}j(\mathbf{q},t) = \left[ \frac{-1}{\alpha(q,0)}(iq)n(\mathbf{q},t) - \gamma\frac{d}{dt}(iq)n(\mathbf{q},t) \right.$$
$$\left. - (iq)U(\mathbf{q},t) \right], \tag{A1}$$

where $\bar{n} = N/A$ is the number density, and $m = M/N$ is the particle mass. The left-hand side is, with some normalization, $M dp/dt$. The terms on the right are the forces from compressibility, the damping term, and the external force from the substrate potential $U$, respectively.

We now use the continuity equation $\nabla j(\mathbf{r}, t) = -dn(\mathbf{r}, t)/dt$, which can be rewritten as $iqj(\mathbf{q}, t) = -dn(\mathbf{q}, t)/dt$. Substituting for $j(\mathbf{q}, t)$ gives a damped harmonic-oscillator equation,

$$\frac{d^2}{dt^2}n(\mathbf{q},t) = \frac{-q^2\bar{n}}{m\alpha(q,0)}n(\mathbf{q},t) - \frac{q^2\bar{n}\gamma}{m}\frac{d}{dt}n(\mathbf{q},t) - \frac{q^2\bar{n}}{m}U(\mathbf{q},t) \tag{A2}$$

$$= -\omega_0^2 n(\mathbf{q},t) - \frac{1}{t_{\mathrm{ph}}^0}\frac{d}{dt}n(\mathbf{q},t) - \omega_0^2\alpha(q,0)U(\mathbf{q},t), \tag{A3}$$

where $\omega_0^2 = q^2\bar{n}/(m\alpha(\mathbf{q},0))$, and the phonon lifetime is $t_{\mathrm{ph}}^0 = m/(\gamma q^2\bar{n})$.

Fourier transforming to the frequency domain, we obtain

$$-\omega^2 n(\mathbf{q},\omega) = -\omega_0^2 n(\mathbf{q},\omega) + \frac{i\omega}{t_{\mathrm{ph}}^0}n(\mathbf{q},\omega)$$
$$- \omega_0^2\alpha(\mathbf{q},0)U(\mathbf{q},\omega). \tag{A4}$$

Now using the relation $n(\mathbf{q},\omega) = -\alpha(\mathbf{q},\omega)U(\mathbf{q},\omega)$, for $\alpha$ we have

$$\alpha(\mathbf{q},\omega) = \frac{\alpha(\mathbf{q},0)}{1 - \dfrac{\omega^2}{\omega_0^2} - i\,\dfrac{\omega}{\omega_0^2 t_{\mathrm{ph}}^0}} \ . \qquad (A5)$$

If we use the result of Eq. (28) in Eq. (13), we see that what has been defined as the phonon lifetime is

$$t_{\mathrm{ph}}(\mathbf{q},\omega) = \frac{m\,\alpha(\mathbf{q},0)}{q^2 \bar{n}} \omega_0^2 t_{\mathrm{ph}}^0 \left[ \left(1 - \frac{\omega^2}{\omega_0^2}\right)^2 + \left(\frac{\omega}{\omega_0^2 t_{\mathrm{ph}}^0}\right)^2 \right]. \quad (A6)$$

In the limit of $\omega^2 \ll \omega_0^2 = q^2 \bar{n}/[m\,\alpha(\mathbf{q},0)]$ and underdamped phonons $(1/t_{\mathrm{ph}} \ll \omega_0)$, we have $t_{\mathrm{ph}} = t_{\mathrm{ph}}^0$.

[1] For a recent overview see the Mater. Res. Soc. Bull. **18**, 15 (1993), or I.L. Singer, in *Dissipative Processes in Tribology, Proceedings of the 20th Leeds-Lyon Symposium on Tribology (1993)*, edited by D. Dowson, C. M. Taylor, T. H. C. Childs, M. Gopdet, and G. Dalmez (Elsevier, New York, 1994).

[2] J. Krim and A. Widom, Phys. Rev. B **38**, 12 184 (1988).

[3] J. Krim, D. H. Solina, and R. Chiarello, Phys. Rev. Lett. **66**, 181 (1991); J. Krim and R. Chiarello, J. Vac. Sci. Technol. A **9**, 2566 (1991).

[4] J. Krim, E. T. Watts, and J. Digel, J. Vac. Sci. Technol. A **8**, 3417 (1990); E. T. Watts, J. Krim, and A. Widom, Phys. Rev. B **41**, 3466 (1990).

[5] M. L. Gee, P. M. McGuiggan, J. N. Israelachvili, and A. M. Homola, J. Chem. Phys. **93**, 1895 (1990).

[6] M. Schöen, C. L. Rhykerd, D. Diestler, and J. H. Cushman, Science **245**, 1223 (1989).

[7] F. Heslot, N. Fraysse, and A. M. Cazabat, Nature **338**, 640 (1989).

[8] P. A. Thompson, G. S. Grest, and M. O. Robbins, Phys. Rev. Lett. **68**, 3448 (1992); J. A. Harrison, R. J. Colton, C. T. White, and D. W. Brenner, Wear **168**, 127 (1993).

[9] P. A. Thompson and M. O. Robbins, Phys. Rev. A **41**, 6830 (1990).

[10] M. Cieplak, E. D. Smith, and M. O. Robbins, Science **265**, 1209 (1994).

[11] L. Sneddon, M. C. Cross, and D. S. Fisher, Phys. Rev. Lett. **49**, 292 (1982).

[12] J. B. Sokoloff, Phys. Rev. B **42**, 760 (1990).

[13] W. Steele, Surf. Sci. **36**, 317 (1973).

[14] *Inert Gases*, edited by M. L. Klein (Springer Verlag, New York, 1984); *Rare Gas Solids*, edited by M. L. Klein and J. A. Venables (Academic, New York, 1976), Vol. 1; J. O. Hirschfelder, C. F. Curtiss, and R. B. Bird, *Molecular Theory of Gases and Liquids* (Wiley, New York, 1954).

[15] Some people have argued that bulk data are better fit by $\epsilon/k_B = 160$ K. Since our results are normalized by $\epsilon$, this distinction is immaterial and has no qualitative effect on our results.

[16] L. W. Bruch and J. M. Phillips, Surf. Sci. **91**, 1 (1980).

[17] J. B. Sokoloff, J. Krim, and A. Widom, Phys. Rev. B **48**, 9134 (1993).

[18] P. A. Thompson, M. O. Robbins, and G. S. Grest, Isr. J. Chem. **35**, 93 (1995).

[19] G. S. Grest and K. Kremer, Phys. Rev. A **33**, 3628 (1986).

[20] Y. Frenkel and T. Kontorova, Zh. Éksp. Teor. Phys. **8**, 89 (1938); **8**, 1340 (1938); **8**, 1349 (1938); F.V. Frank and van der Merwe, Proc. R. Soc. London Ser. A **198**, 205 (1949); J.E. Sacco and J.B. Sokoloff, Phys. Rev. B **18**, 6549 (1978); G.M. McClelland, in *Springer Series in Surface Sciences, Vol. 17, Adhesion and Friction*, edited by M. Grunze and H.J. Kreuzer (Springer-Verlag, Berlin, 1989).

[21] M. Hirano and K. Shinjo, Wear **168**, 121 (1983); Surf. Sci. **283**, 473 (1983).

[22] See Fig. 2 and the discussion in Ref. 10 for temperature variation data.

[23] B. N. J. Persson, in *Computations for the Nano-Scale*, Vol. 240 of *NATO Advanced Study Institute Series E: Applied Sciences*, edited by P. E. Blochl, C. Joachim, and A. J. Fisher (Kluwer, Dordrecht, 1993), p. 21.

[24] S.N. Coppersmith and D.S. Fisher, Phys. Rev. B **28**, 2566 (1983).